Phenotype Driven Analysis of Whole Genome Sequencing Identifies Deep Intronic Variants that Cause Retinal Dystrophies by Aberrant Exonization

Matteo Di Scipio, Erika Tavares, Shriya Deshmukh, Isabelle Audo, Kit Green-Sanderson, Yuliya Zubak, Fayçal Zine-Eddine, Alexander Pearson, Anjali Vig, Chen Yu Tang, et al.

HAL Id: hal-02940524

https://hal.sorbonne-universite.fr/hal-02940524

Submitted on 16 Sep 2020

Genetics

Phenotype Driven Analysis of Whole Genome Sequencing Identifies Deep Intronic Variants that Cause Retinal Dystrophies by Aberrant Exonization

Matteo Di Scipio,[1] Erika Tavares,[1] Shriya Deshmukh,[1] Isabelle Audo,[2–4]
Kit Green-Sanderson,[1] Yuliya Zubak,[1] Fayçal Zine-Eddine,[1] Alexander Pearson,[1] Anjali Vig,[1]
Chen Yu Tang,[1] Antonio Mollica,[1] Jonathan Karas,[1] Anupreet Tumber,[5] Caberry W. Yu,[1]
Gail Billingsley,[1] Michael D. Wilson,[1,6] Christina Zeitz,[2] Elise Héon,[1,5,7] and Ajoy Vincent[1,5,7]

[1]Genetics and Genomic Biology, The Hospital for Sick Children, Toronto, Canada
[2]Sorbonne Université, INSERM, CNRS, Institut de la Vision, Paris, France
[3]CHNO des Quinze-Vingts, INSERM-DGOS CIC1423, Paris, France
[4]University College London Institute of Ophthalmology, London, United Kingdom
[5]Department of Ophthalmology and Vision Sciences, The Hospital for Sick Children, Toronto, Canada
[6]Department of Molecular Genetics, University of Toronto, Toronto, Canada
[7]Department of Ophthalmology and Vision Sciences, University of Toronto, Toronto, Canada

PURPOSE. To demonstrate the effectiveness of combining retinal phenotyping and focused variant filtering from genome sequencing (GS) in identifying deep intronic disease causing variants in inherited retinal dystrophies.

METHODS. Affected members from three pedigrees with classical enhanced S-cone syndrome (ESCS; Pedigree 1), congenital stationary night blindness (CSNB; Pedigree 2), and achromatopsia (ACHM; Pedigree 3), respectively, underwent detailed ophthalmologic evaluation, optical coherence tomography, and electroretinography. The probands underwent panel-based genetic testing followed by GS analysis. Minigene constructs (*NR2E3*, *GPR179* and *CNGB3*) and patient-derived cDNA experiments (*NR2E3* and *GPR179*) were performed to assess the functional effect of the deep intronic variants.

RESULTS. The electrophysiological findings confirmed the clinical diagnosis of ESCS, CSNB, and ACHM in the respective pedigrees. Panel-based testing revealed heterozygous pathogenic variants in *NR2E3* (NM_014249.3; c.119-2A>C; Pedigree 1) and *CNGB3* (NM_019098.4; c.1148delC/p.Thr383Ilefs*13; Pedigree 3). The GS revealed heterozygous deep intronic variants in Pedigrees 1 (*NR2E3*; c.1100+1124G>A) and 3 (*CNGB3*; c.852+4751A>T), and a homozygous *GPR179* variant in Pedigree 2 (NM_001004334.3; c.903+343G>A). The identified variants segregated with the phenotype in all pedigrees. All deep intronic variants were predicted to generate a splice acceptor gain causing aberrant exonization in *NR2E3* [89 base pairs (bp)]*, GPR179* (197 bp), and *CNGB3* (73 bp); splicing defects were validated through patient-derived cDNA experiments and/or minigene constructs and rescued by antisense oligonucleotide treatment.

CONCLUSIONS. Deep intronic mutations contribute to missing heritability in retinal dystrophies. Combining results from phenotype-directed gene panel testing, GS, and in silico splice prediction tools can help identify these difficult-to-detect pathogenic deep intronic variants.

Keywords: *NR2E3*, *GPR179*, *CNGB3*, RNA splice sites, introns, deep intronic variant, antisense oligonucleotides, enhanced S-cone syndrome, congenital stationary night blindness, color vision defects, achromatopsia, retinal dystrophies

Inherited retinal dystrophies (IRDs) are a leading cause of childhood blindness for which over 250 genes have been identified (RetNet, https://sph.uth.edu/retnet/). As we have entered the era of gene-specific patient management, there is increased incentive to clarify the genetic diagnosis of patients. Panel-based next generation sequencing (NGS) techniques primarily focus on detecting exonic and canonical splicing variants with a mutation detection rate of 60% to 70%. [1] The mutation detection rate is different among various clinical classes of IRDs; it exceeds 90% in single-gene disorders (e.g., *RS1* and *CHM*) and some well-defined forms of IRDs (e.g., achromatopsia [ACHM] and congenital stationary night blindness [CSNB]), but it is much lower in sporadic retinitis pigmentosa (<60%) and central

areolar choroidal dystrophy (35%).[2] In a growing number of unsolved IRD cases it is becoming clear that the missing heritability is found in the intronic regions of known genes, such as *ABCA4*, *CEP290*, *USH2A*, *CLRN1*, *CNGB3* and *CACNA1F*.[3–9] In these instances, a distinct phenotype or the presence of a heterozygous disease-causing variant in a known autosomal recessive (AR) gene initiated a comprehensive analysis of the noncoding regions of the gene of interest to uncover novel deep-intronic disease causing variants.

Intronic variants have the potential to result in missplicing pre-mRNA and generate an aberrant transcript that could be disease causing in some IRD cases. This can occur where cis-splicing motif sequences are gained or cryptic splice sites in an intron are activated.[10] Common splice sites include 5′ donor sites, 3′ acceptor sites, branch point and polypyrimidine tract sequences, and splicing silencer or enhancer regions.[11] Although most of these intronic variants are well tolerated, some of them have the potential to alter correct splicing through the creation or disruption of motifs read by the spliceosome.[12] This can create a frameshift or a premature termination codon that can lead to nonsense mediated decay.[13]

In this study, we combined phenotyping with NGS-based analysis of the noncoding intronic regions of genes of interest to uncover pathogenic deep intronic variants in three AR IRDs, enhanced S-cone syndrome [(ESCS; *NR2E3*) (OMIM: 604485)],[14] complete CSNB ([cCSNB; *GPR179*] [OMIM: 614515]),[15,16] and ACHM ([*CNGB3*] [OMIM: 605080]).[17] Functional validation of the intronic variants were performed using patient-derived cDNA analysis and/or minigene constructs incorporating the deep intronic variants and antisense oligonucleotide rescue treatments.

MATERIALS AND METHODS

Patient-related

This project was approved by the Ethics Review Board at the Hospital for Sick Children, Toronto, and met the Tenets of the Declaration of Helsinki. Family members across three pedigrees were recruited at the Hospital for Sick Children after obtaining informed consent; this included three members from Pedigree 1 (ESCS; proband and unaffected parents; Fig. 1A), seven members from Pedigree 2 (cCSNB; proband, four unaffected siblings and unaffected parents; Fig. 2A) and five members from Pedigree 3 (ACHM; proband, two affected siblings and unaffected parents; Fig. 3A). The ocular phenotype was defined in all affected individuals by assessing various parameters of visual function and structure [(best corrected visual acuity (BCVA), color (Hardy Rand Rittler Charts) and contrast vision, fundus photography, spectral-domain optical coherence tomography (SD-OCT; Zeiss Cirrus (Pedigrees 1 and 2) or Heidelberg Spectralis (Pedigree 3)) and an International Society for Clinical Electrophysiology of Vision standard full-field electroretinogram (ERG)[18]]. All unaffected members in Pedigree 2 (parents and siblings) underwent eye examinations including ERG. DNA was extracted from all participants for segregation analysis. All probands, as well as affected siblings in Pedigree 3, underwent candidate gene panel testing through the clinic (details in Supplementary Table S1). Fibroblast or lymphoblast cell lines were established from each proband for RNA extraction.

Genome Sequencing and Variant Analysis

Genome sequencing (GS) was performed in five subjects at The Center for Applied Genomics (TCAG) as previously published.[19,20] Briefly, paired-end (2 × 150 base pairs [bp]) sequencing was performed on the three probands, one unaffected sibling in Pedigree 2 (II-3, Fig. 2A) and one affected sibling in Pedigree 3 (II-2, Fig. 3A) using Illumina Hi-Seq X platform and the reads were mapped to the GRCh37 reference sequence using bwa-mem v0.7.12.[21] Duplicate reads were removed using MarkDuplicates Picard v2.5.0 (https://broadinstitute.github.io/picard/). Local read realignment and variant calling were accomplished using GATK v3.7.0, and calls were annotated using ANNOVAR.[22,23] Mobile transposable element (TE) insertion analysis was performed with Mobster v0.2.4.1.[24] Copy number variants were called using ERDS v1.1 and CNVnator v0.3.2 using a window size of 500 bp.[25,26]

From the pedigree information and clinical diagnoses, an AR mode of inheritance was assumed in each family. Variant analyses were performed using both candidate gene panel and genome wide approaches utilizing previously published customized pipelines, and included multiple *in silico* prediction tools and control population databases.[19,27,28] Prioritization of variants was established by variant frequency, gene relevance, pathogenicity scores, and segregation analysis. Supplementary Figures S1 to S3 details the candidate gene filtering approach, genome wide filtering approach, and variant prioritization in each pedigree. Segregation analysis was performed using the primer pairs 2, 9 and 13 for *NR2E3*, *GPR179* and *CNGB3*, respectively (Supplementary Tables S2–S4).

In Silico Splice Prediction of Intronic Variants

The gain or loss of potential donor or acceptor sites in a 200 bp window around candidate variant sites were tested in silico using four splice prediction algorithms (SpliceSiteFinder, MaxEntScan, NNSPLICE, and GeneSplicer)[29–32] implemented through Alamut Visual Software (https://www.interactive-biosoftware.com/alamut-visual/). Scores that met preset thresholds in three or more algorithms were flagged as significant (Table 1). SpliceAI (Illumina) prediction software was also used to assess aberrant splicing of rare intronic variants in candidate genes.[33]

Splicing Reporter Minigene Constructs, HEK293T Cell Transfection and RT-PCR

NR2E3 and *GPR179* minigene constructs were developed using similar techniques as previously described.[34–36] The respective proband's genomic DNA was amplified by polymerase chain reaction (PCR) using the primer pairs 1 (*NR2E3*) and 8 (*GPR179*) (Supplementary Tables S2 and S3). The primer pairs were located in the region complementary to introns 6 and 8 for *NR2E3*, and introns 1 and 4 for *GPR179*. The 5′ end of the forward and reverse primers were designed to include a HindIII site and SalI site, respectively, to facilitate plasmid cloning by restriction enzyme digest. Subsequent PCR amplification product was purified using QIAEX II Gel Extraction Kit. The purified DNA amplicon (3 μg) was double digested using HindIII-HF, SalI-HF and 10X CutSmart Buffer according to manufacturer's instructions (New England Biolabs Cloner); the peGFP-N1 plasmid vector was also double digested separately using identical protocol.
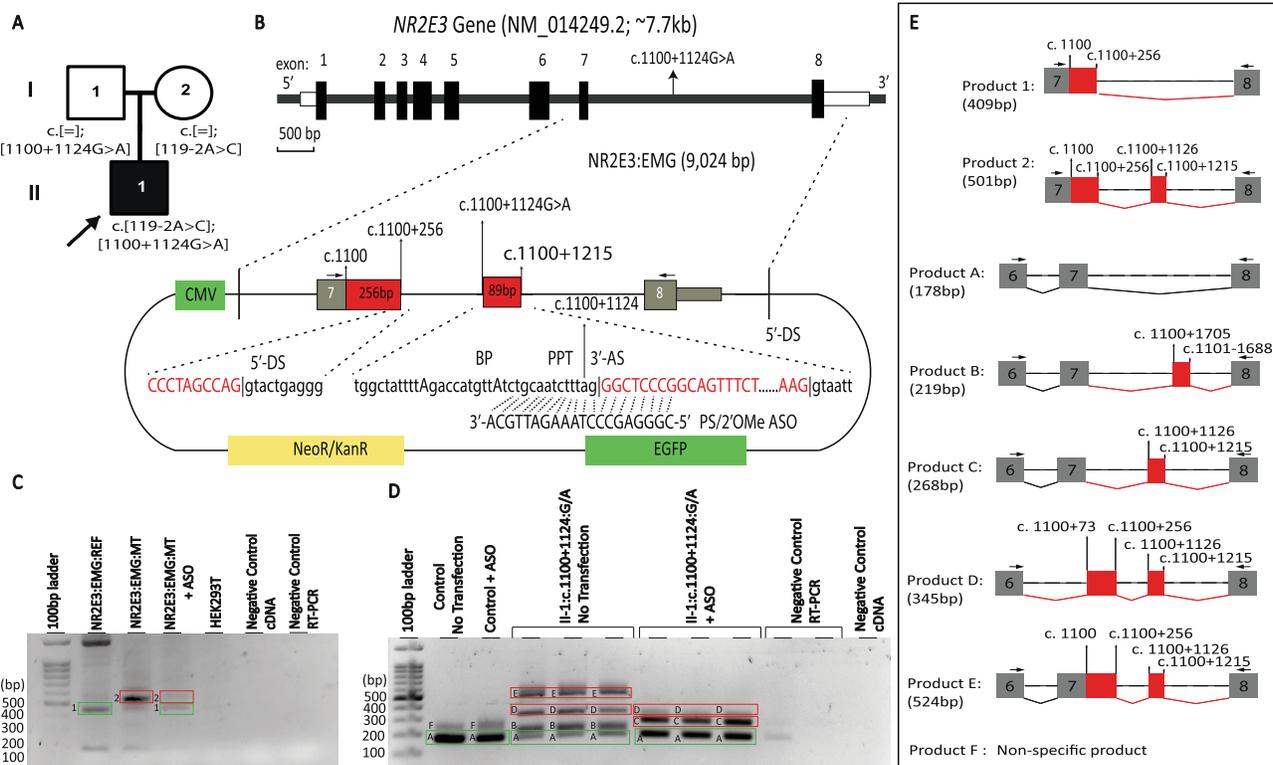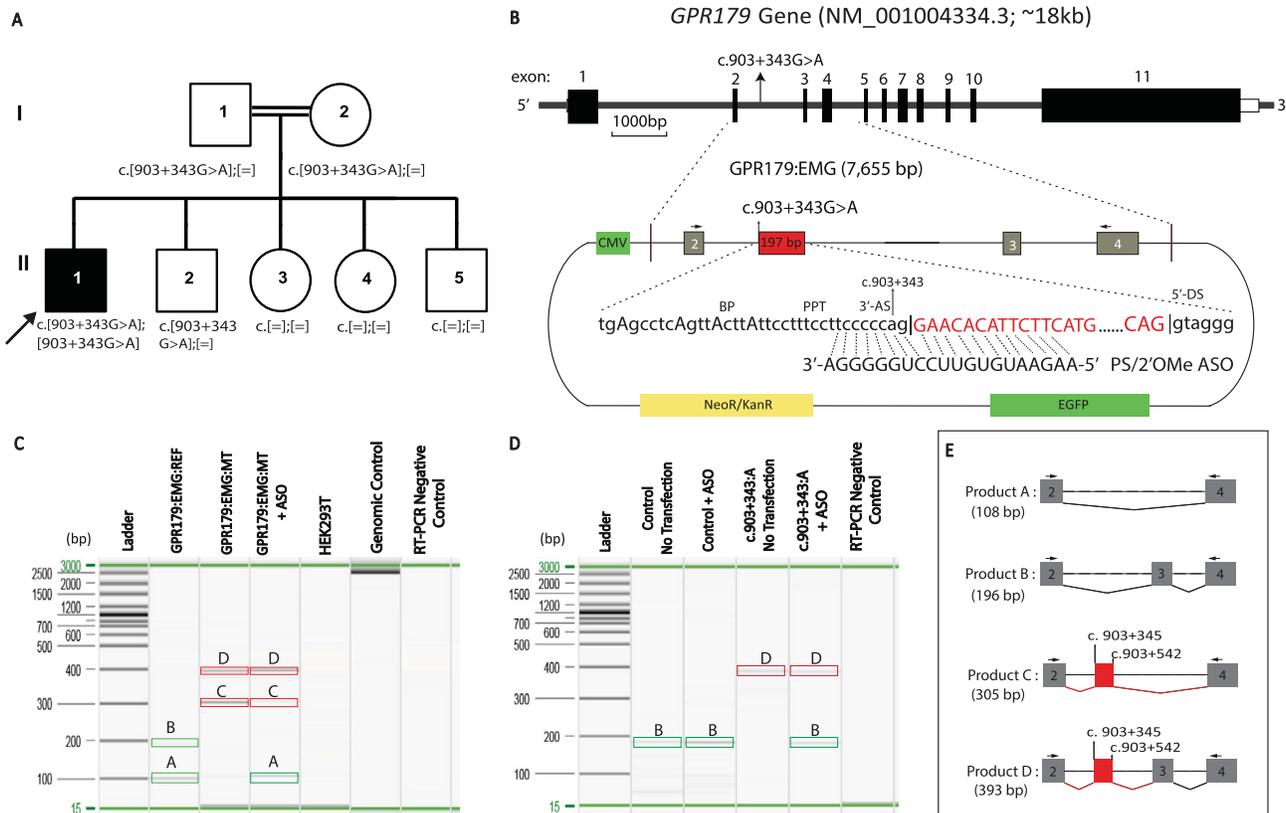
FIGURE 1. Segregation of the *NR2E3* variants and the functional validation of the deep intronic variant (c.1100+1124G>A) in Pedigree 1. (**A**) Pedigree structure and segregation results for *NR2E3*. (**B**) A schematic representation of *NR2E3* and the location of the deep intronic variant (c.1100+1124G>A) in the *top panel*; *bottom panel* schema includes minigene construct, sequences around gained splice sites, the ASO sequence and its binding site. (**C**) RT-PCR of HEK293T cells transfected with minigenes: reference construct (NR2E3:EMG:REF; c.1100+1124:G) displayed product 1 [409 bp, reference transcript], the variant construct (NR2E3:EMG:MT; c.1100+1124:A) displayed a larger product 2 (501 bp, aberrant transcript), and after ASO treatment (NR2E3:EMG:MT + ASO_{NR2E3)}, there was diminished amount of product 2. *Green boxes* denote reference transcripts and ASO-recovered reference transcripts. *Red boxes* denote aberrant transcripts. (**D**) RT-PCR results from control and patient-derived fibroblast cell lines with and without transfection of ASO_{NR2E3}. Control fibroblasts demonstrated product A (178 bp, reference transcript) and a nonspecific product F. Patient-derived fibroblasts demonstrated four distinct bands (products A, B, D and E); product A represents reference transcript as a result of leakage of the two splice mutations in the proband, products D (345 bp) and E (524 bp) are two aberrant splice products as a result of the deep intronic variant, and product B (219 bp) is likely an alternatively misspliced transcript. Treatment with ASO_{NR2E3} in the patient fibroblasts reduced the relative levels of products D and E (aberrant splice products) and increased the level of normal transcript (product A); it is noted that a new aberrantly spliced product using the deep intronic splice acceptor gain site (product C, 268 bp) was observed. *Green boxes* denote reference transcripts. *Red boxes* denote aberrant transcripts. (**E**) Schematic representation of the cDNA products obtained in **C** and **D**. AS, acceptor site; BP, branch point sequence; CMV, cytomegalovirus promoter; DS, donor site; EGFP, enhanced green fluorescent protein; NeoR/KanR, neomycin/kanamycin resistance; PPT, polypyrimidine tract; PS/2′OMe, phosphorothioate/2′O Methyl.

TABLE 1. *In Silico* Splice Predictions

Variant (gene; transcript; position)	Acceptor Site Gain	SSF [0-100]	MaxEnt [0-16]	NNSPLICE [0-1]	GeneSplicer [0-15]	SpliceAI [0-1]	Donor Site Gain (SpliceAI)
NR2E3; NM_014249.3; c.1100+1124G>A; g.17:71815241G>A	Position: c.1100+1126	78.36	7.47	0.88	1.67	0.63	Position: c.1100+1214
GPR179; NM_001004334.3; c.903+343G>A; g.15:36494957C>T	Position: c.903+345	90.61	12.24	0.97	9.91	0.86	Position: c.903+542
CNGB3; Transcript NM_019098.4; c.852+4751A>T; g.8:87674402T>A	Position: c.852+4756	83.92	8.08	-	5.97	0.60	Position: c.852+4829

In silico splice prediction scores using Alamut Visual Software included SSF, MaxEnt, NNSPLICE, and GeneSplicer flagged these deep intronic mutations as pathogenic acceptor gain mutations when greater than the default threshold values (SSF ≥70, MaxEnt ≥0, NNSPLICE ≥0.4, GeneSplicer ≥0, SpliceAI ≥0.5). SpliceAI (Illumina) also flagged these mutations as a pathogenic acceptor gain score. These scores also provided predicted aberrant exonization start and end positions. Genomic coordinates refer to the build GRCh37/hg19 for *GPR179* and *CNGB3*, and GRCh38/hg38 for *NR2E3*.
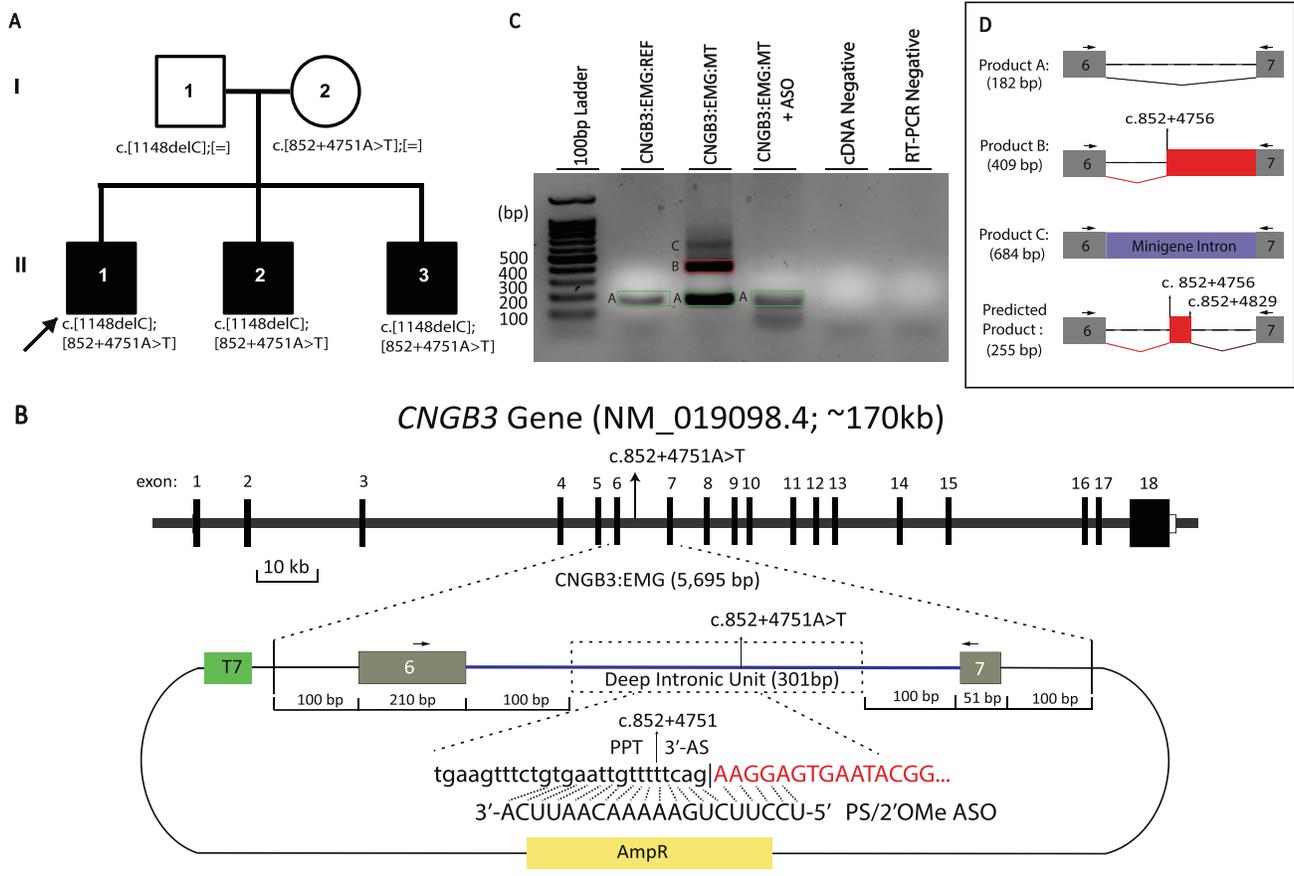
FIGURE 2. Segregation analysis in Pedigree 2 and the functional validation of the *GPR179* deep intronic variant (c.903+343G>A). (**A**) Pedigree structure and segregation results for the *GPR179* variant. (**B**) Top panel depicts a schematic representation of *GPR179* and the location of the deep intronic variant (c.903+343G>A); *bottom panel* schema includes minigene construct, sequences around gained splice sites, and the ASO sequence and its binding site. (**C**) RT-PCR of HEK293T cells transfected with minigene reference construct (GPR179:EMG:REF; [c.903+343:G]) displayed two products (A and B, 108 and 196 bp, respectively, reference transcripts) and the variant construct (GPR179:EMG:MT; c.903+343:A) displayed two larger splice products that used the novel splice acceptor site (C and D, 305 and 393 bp, respectively, aberrant transcripts); following ASO treatment (GPR179:EMG:MT + ASO$_{GPR179}$) there was relative reduction in the levels of product C, retained product D and rescue of product A. Green boxes denote reference transcripts. Red boxes denote aberrant transcripts. (**D**) RT-PCR results from control and patient-derived lymphoblast cell lines with and without transfection of ASO$_{GPR179}$. Control lymphoblasts demonstrated product B (reference transcript); patient-derived lymphoblasts demonstrated product D (aberrant transcript) and on treatment with ASO$_{GPR179}$ product D was still detected, but there was recovery of reference transcript (product B). Green boxes denote reference transcripts. Red boxes denote aberrant transcripts. (**E**) Schematic representation of the cDNA products obtained in **C** and **D**. AS, acceptor site; BP, branch point sequence; CMV, cytomegalovirus promoter; DS, donor site; EGFP, enhanced green fluorescent protein; NeoR/KanR, neomycin/kanamycin resistance; PPT, polypyrimidine tract; PS/2′OMe, phosphorothioate/2′O methyl.

T4 DNA Ligase was used to deliver the amplicon into the vector peGFP-N1 backbone containing a cytomegalovirus promoter (Clontech, TakaRa, Figs. 1B, 2B) in a 3:1 molar ratio of insert to vector. The ligated product was transformed into One Shot TOP10 chemically competent *Escherichia coli* (ThermoFisher Scientific, Waltham, MA, USA). Kanamycin was used for clone selection; selected clones were grown in 5ml LB medium containing 250 µg of kanamycin and incubated at 37° C and 225 rpm for 24 hours. The plasmid DNA from each incubated colony was purified using the QIAprep Spin Miniprep kit. On Sanger sequencing, the minigene clones were confirmed to only include mutant constructs. The constructs were labeled NR2E3:EMG:MT (9,024 bp) and GPR179:EMG:MT (7,655 bp), respectively. To generate reference constructs, site-directed mutagenesis of NR2E3:EMG:MT and GPR179:EMG:MT clones were conducted using repliQa HiFi Assembly Mix (Quantabio, Beverly, MA, USA) and Q5 Site-Directed Mutagenesis Kit (New England Biolabs, Ipswich, MA, USA), respectively, according to manufacturer's guidelines.[37,38] Primer pairs 4

and 11 that contained normal reference nucleotide at the variant site for *NR2E3* and *GPR179*, respectively, were used for this purpose (Supplementary Tables S2 and S3). The resulting colonies' plasmid DNA was purified using the QIAprep Spin Miniprep kit. On Sanger sequencing, a clone with the reference construct was chosen; the constructs were labeled NR2E3:EMG:REF and GPR179:EMG:REF, respectively.

To validate the aberrant splicing of the *CNGB3* variant, a 962bp DNA fragment (gBlock) was designed and synthesized by GeneArt Strings (ThermoFisher Scientific, Waltham, MA, USA). This fragment contained exon 6 with flanking introns, connected to a unit of intron 6 containing the deep intronic variant with flanking intronic regions (169 bp and 131 bp, respectively), which connects to exon 7 with flanking introns (refer to Fig. 3B for details). A DNA fragment containing the normal reference nucleotide at the intronic variant site and another containing the mutant intronic variant were synthesized (Supplementary Table S5). The reference and variant design sequences were tested using

FIGURE 3. Segregation analysis in Pedigree 3 and the functional validation of the *CNGB3* deep intronic variant (c.852+4751A>T). (**A**) Pedigree structure and segregation analysis for the *CNGB3* variants. (**B**) Top panel depicts a schematic representation of *CNGB3* and the location of the deep intronic variant (c.852+4751A>T); bottom panel schema includes minigene construct, sequences around gained splice sites, ASO sequence and its binding site. (**C**) RT-PCR of HEK293T cells transfected with minigene reference construct (CNGB3:EMG:REF) displayed product A (182 bp, reference transcript), and the variant construct (CNGB3:EMG:MT) displayed products A (reference transcript due to leakage), B (409 bp, aberrant transcript), and C (684 bp; unspliced minigene); following ASO treatment (CNGB3:EMG:MT + ASO$_{CNGB3}$), there was abrogation of the aberrant transcript (product B) with presence of reference transcript (product A). (3D) Schematic representation of the cDNA products obtained in **C**. AmpR, ampicillin resistance; AS, acceptor site; PPT, polypyrimidine tract; PS/2′OMe, phosphorothioate/2′O Methyl; T7, T7 promoter.

all of the splice prediction algorithms (described earlier) to ensure no new splice sites were created or destroyed. The DNA product was then blunt-end cloned using Clone-JET PCR Cloning Kit (Invitrogen, Carlsbad, CA, USA) and subsequently transformed into One Shot TOP10 chemically competent *E. coli* (Thermo Fisher Scientific). Ampicillin was used for clone selection; selected clones were grown in 5 mL LB medium containing 250 µg of ampicillin and incubated at 37°C and 225 rpm for 24 hours. Randomly selected colonies for the reference and mutant constructs underwent plasmid DNA purification using the QIAprep Spin Miniprep Kit. DNA plasmid sequencing identity and fidelity was confirmed on Sanger sequencing. The reference and mutant minigene constructs (5695 bp long) were labeled CNGB3:EMG:REF and CNGB3:EMG:MT, respectively. Primers used for clone validation are listed in Supplementary Table S4. Similar modified minigene designs using shortened introns have been published.[8,39]

HEK293T cells were cultured in DMEM (Gibco, Gaithersburg, MD, USA) with 10% fetal bovine serum (FBS) added. For HEK293T cell transfection with clones of minigene constructs, 2.5 µg of the vector was added in a mixture of 250 µL Opti-MEM serum-free medium (Gibco, Gaithersburg, MD, USA) and 7.5 µL X-tremeGENE HP DNA Transfection Reagent (Roche, Basel, Switzerland) and incubated for 25 minutes at room temperature to form a stable complex; this was then pipetted into a 6-well plate and incubated at 37°C for 72 hours. Similar techniques were used for all six minigene constructs (one reference and mutant construct per gene).

RNA was isolated using the RNeasy Mini Kit (Qiagen, Hilden, Germany). The cDNA synthesis was conducted with Superscript IV One-Step RT-PCR System (Invitrogen) using equivalent RNA amounts (40ng each) in a 20µL reaction. Primer pairs 3, 10, and 16 were used for minigene splice detection for *NR2E3* (Platinum SuperFi PCR mastermix), *GPR179* (Amplitaq Gold 360 Master Mix, Invitrogen) and *CNGB3* (AllTaq Master Mix Kit, Qiagen), respectively (listed in Supplementary Tables S2–S4).

Patient-derived Cell Culture Experiments

Patient-derived fibroblasts (*NR2E3*) were cultured in AMEM (Wisent Bio Products) with 10% FBS added. Patient-derived

TABLE 2. Phenotype Summary of All the Cases

	Pedigree 1 (Proband)	Pedigree 2 (Proband)	Pedigree 3 (Proband)	Pedigree 3 (II-2)	Pedigree 3 (II-3)
Gene (Variants)	*NR2E3*: c.[119-2A>C]; [1100+1124G>A]	*GPR179*: c.[903+343G>A]; [903+343G>A]	*CNGB3*: c.[1148delC]; [852+4751 A>T]		
Symptoms	Nyctalopia at 3 years	Right exotropia – infancy	Nystagmus – infancy Photophobia - infancy	Nystagmus – infancy Photophobia - infancy	Nystagmus – infancy Photophobia - infancy
		Nyctalopia at 11 years			
Age at Recent visit	17 years	17 years	23 years	19 years	14 years
Visual Acuity (Right Eye : Left Eye)	20/25: 20/25	20/70: 20/40	20/200: 20/200	20/160: 20/200	20/200: 20/250
Contrast Sensitivity	1.50: 1.50	1.65:165	0.75:0.60	0.75:0.60	0.75:0.75
Color vision	Moderate RG defect	normal	Strong RG & BY deficit	Strong RG & BY deficit	Strong RG & moderate BY deficit
Refractive error	+0.75+0.50 × 10:	−7.75+1.50 × 108:	−10.50/+4.00 × 105:	−11.00 : −11.00	−8.50/+1.25 × 115:
(Right Eye : Left Eye)	+1.50	−7.75+1.50 × 70	−10.50/+4.00 × 75		−8.00/+1.00 × 70
Retinal exam (Both Eyes)	white dots ST arcade	Tilted disc; tessellated background; dull FR	Macular atrophy	Peripapillary atrophy; dull FR; peripheral lattice OD	Tilted disc; dull FR; peripheral lattice
Fundus Autofluorescence (Both Eyes)	Hypo AF along ST arcade; hyper AF dots periphery	NA	Foveal hyper-AF	Foveolar hypo AF; parafoveal hyper AF	Subtle foveal hyper AF
Optical Coherence Tomography (Both Eyes)	Normal CRT; ONL and OPL rosettes with thick and disorganized retina in mid-periphery	Normal CRT and lamination	Grade 1 FH; Mild disruption of OS in central sub-foveal region	Grade 1 FH; Mild disruption of OS in central sub-foveal region	Grade 1 FH; Mild disruption of OS in central sub-foveal region

AF, autofluorescence; BY, blue-yellow; CRT, central retinal thickness; FH, foveal hypoplasia; FR, foveal reflex; NA, not available; ONL, outer nuclear layer; OPL, outer plexiform layer; OS, outer segments; RG, red-green; ST, superotemporal.

lymphoblasts (*GPR179* and *CNGB3*) were cultured with RPM1 1640 medium (Gibco). For *NR2E3*, a nested PCR approach was used with 120ng of cDNA as the ectopic expression of this gene is low in fibroblasts (Primer pairs 6 and 7 in Supplementary Table S2; PCR conditions available on request). For *GPR179*, 200ng cDNA was used for reverse transcriptase (RT)-PCR in an Amplitaq Gold 360 Master Mix (primer pair 10 in Supplementary Table S3; PCR conditions available on request).

Antisense Oligonucleotides Design and Rescue Experiments

Antisense oligonucleotides (ASO) were designed as a 20 bp sequence that would be complementary with a sequence that overlaps the deep intronic variant of interest in *NR2E3*, *GPR179,* and *CNGB3*, thereby acting as steric spliceosome inhibitors.[40] A phosphorothioate (PS) backbone linkage was chosen so as to increase nuclease resistance and half-life.[41] Each nucleotide ribose in the primer sequence was designed (Integrated DNA Technologies, Iowa) to contain a 2′O-Me modification to prevent RNAaseH pathway degradation of the transcript.[41] ASOs used in this study were primers 5, 12, and 14 (Supplementary Tables S2–S4).

HEK293T cells were co-transfected with mutant minigene constructs (2.5 µg) and ASO (final culture concentration of 200nM). For transfection of ASOs in patient-derived fibrob-

lasts or lymphoblasts, appropriate volume of ASO was added to reach a final concentration of 5 µmol/L. Transfection and RT-PCR were performed as previously described in earlier sections of the methods.

Electrophoresis and Imaging Techniques

The splicing assays for *NR2E3* and *CNGB3* (patient derived cDNA and/or minigene RT-PCR) were performed by agarose gel electrophoresis (1.5%) and imaged using ChemiDoc Imaging system (Bio-Rad, Hercules, CA, USA). The splicing assays for *GPR179* were performed using high-resolution capillary electrophoresis where a digital image was generated (QIAxcel Advanced system; Qiagen).

RESULTS

Pedigree 1 (Enhanced S-Cone Syndrome)

Clinical Phenotype and Genetic Results. The proband, a male child of North European ancestry, had complaints of night blindness since three years of age. At 11 years, his BCVA was 20/25 in both eyes and had a strong red-green color deficit (Table 2). Retinal examination showed a few faint white dots along the superotemporal arcades but was otherwise unremarkable (Fig. 4A). The SD-OCT showed no evidence of foveal schisis, but there were retinal
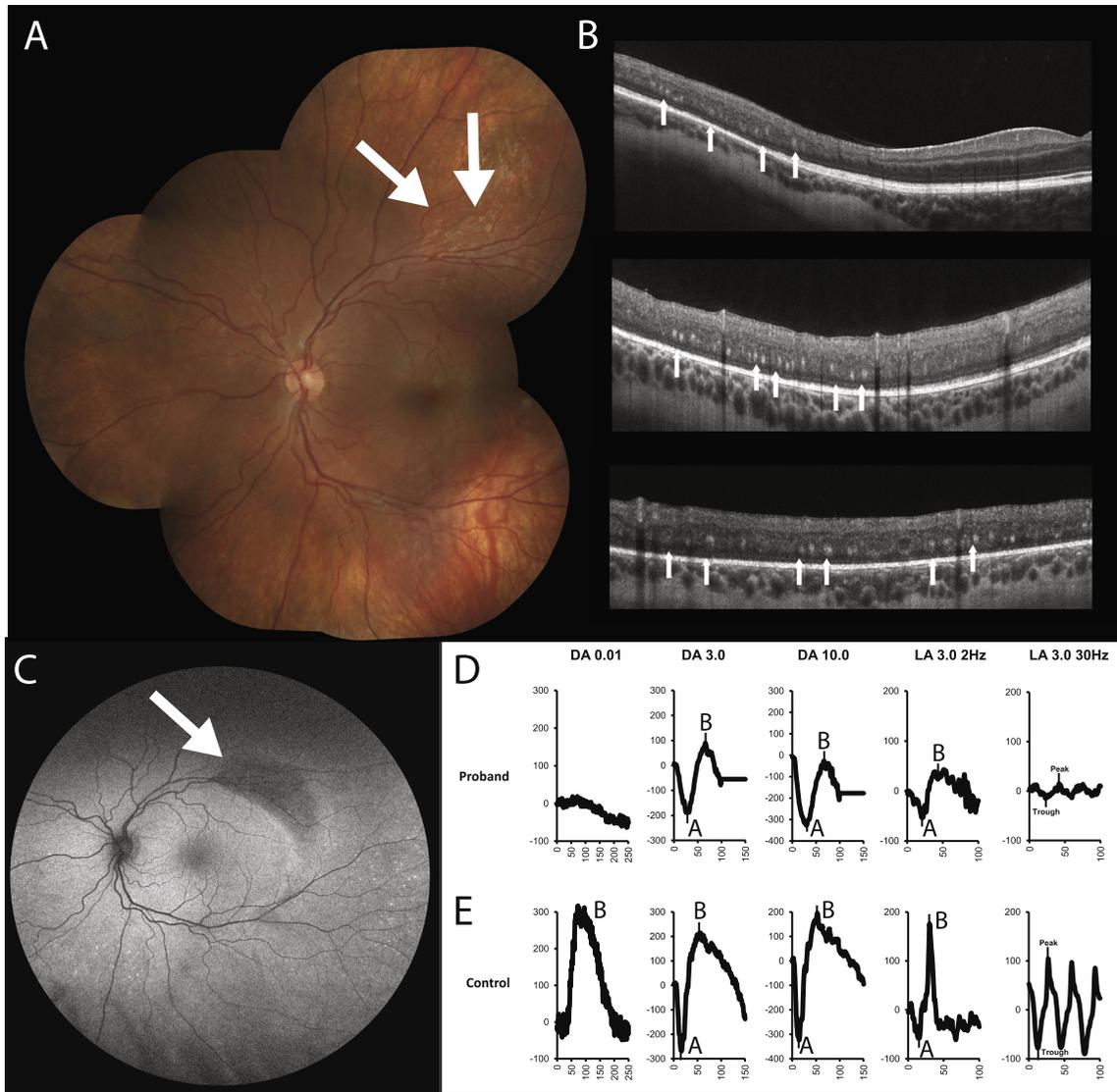
Figure 4. Clinical phenotype of Pedigree 1 proband (II-1). (**A**) Fundus image from the left eye is largely unremarkable except for the presence of a few deep retinal white dots along the superotemporal arcade (*white arrows*). (**B**) SD-OCT images from the right (2 images; top – *horizontal line* scan across temporal macula; middle – *horizontal line* scan above superotemporal arcade in the region of *white dots*) and left eyes (bottom image – *vertical line* scan temporal to macula), respectively. All three images show presence of rosettes in the region of outer nuclear and plexiform layers (*white arrows*); marked disruption of retinal lamination was observed in the middle and outer retina in the region of the rosettes but the retinal thickness appeared increased in these regions. The macular retinal thickness and lamination was largely preserved. (**C**) Fundus autofluorescence image of the left eye shows hypofluorescence (*white arrow*) corresponding to the region of white dots along superotemporal arcade in **A**. In addition, there were multiple hyper autofluorescent dots in the periphery. (**D**) ERG from the proband showed nondetectable dark adapted (DA) dim light response (DA 0.01 ERG); DA 3.0 and DA 10.0 responses showed markedly reduced a- and b-waves, which are markedly delayed and demonstrated a simplified waveform morphology. The flicker responses showed delayed peak times and markedly reduced amplitudes; the flicker amplitudes were smaller than light adapted (LA) 3.0 2Hz a-wave. The LA 3.0 ERG waveforms were markedly delayed, and resembled DA 3.0 ERGs. The ERG findings are characteristic for enhanced S-cone syndrome. (**E**) ERG responses from a control subject.

rosettes in the outer nuclear and plexiform layers outside the macula; these regions showed retinal thickening and disorganization of middle and inner retinal layers (Fig. 4B). The ERG showed pathognomonic features of ESCS[42] (nondetectable dim-light scotopic response; simplified, delayed and reduced scotopic response to a standard flash that was largely similar in morphology to the photopic standard flash response; and a markedly reduced photopic flicker response; Fig. 4D); control traces are shown in Figure 4E. At 13 years, wide-field autofluorescence (AF) revealed atrophy along the superotemporal arcades, and there were hyper-autofluorescent dots in the periphery (Fig. 4C). Panel-based testing identified a heterozygous previously reported *NR2E3* mutation (c.119-2A>C) leading to skipping of exon 2[14,43]; no variants were found in *NRL*. No copy number variations (CNV) were found when screening *NR2E3*.

GS analysis of the candidate genes revealed two variants in *NR2E3*; the previously identified pathogenic splice variant (c.119-2A>C) and a novel deep intronic variant in intron 7 (chr15: 71815241:G>A; c.1100+1124G>A;

NM_014249.3; GRCh38/hg38). The deep intronic variant was not observed in any GS control databases [gnomAD (https://gnomad.broadinstitute.org/); BRAVO (https://bravo.sph.umich.edu/freeze5/hg38/)]. All in silico tools (Table 1) strongly predicted the gain of a splice acceptor site 2 bp downstream (c.1100+1126), and SpliceAI predicted an aberrant exon of 89 bp with a specific start and stop site. Genotyping showed that the variants segregated with the disease phenotype (Fig. 1A). A detailed analysis of GS did not reveal any other candidate gene with biallelic exonic or canonical splice variants (Supplementary Fig. S1).

Splicing Reporter Minigene RT-PCR and ASO Rescue. HEK293T cells were transfected with the NR2E3:EMG:REF (reference sequence, c.1100+1124:G), NR2E3:EMG:MT (variant sequence, c.1100+1124:A), and NR2E3:EMG:MT + ASO$_{NR2E3}$. After RT-PCR, the reference clone (c.1100+1124:G) displayed a distinct favored band (product 1; 409 bp) whereas the variant clone (c.1100+1124:A) displayed a larger band (product 2; 501 bp); Sanger sequencing confirmed product 2 to have incorporated the aberrant exon of 89 bp (Figs. 1C, 1E). The aberrant exon size and the start sites were as predicted by SpliceAI (Table 1; Fig. 1E). The variant clone cotransfected with ASO$_{NR2E3}$ resulted in diminished amounts of mutant mRNA (product 2), although no increase in reference transcript (product 1) was visible (Fig. 1C). HEK293T cells with no transfection displayed no bands because they do not express *NR2E3*. It is noted that both reference and variant constructs used a different donor site at exon 7 boundary than predicted (Fig. 1E).

Fibroblast RT-PCR and ASO Rescue. In control fibroblasts and ASO$_{NR2E3}$ transfected control fibroblasts product A (178 bp; Fig. 1D) was detected; Sanger sequencing confirmed normal splicing of exon 7 and exon 8. In patient fibroblasts compound heterozygous for c.1100+1124G>A and c.119-2A>C variants, four different transcripts [products A (178 bp), B (219 bp), D (345 bp) and E (524 bp)] were identified (Fig. 1D). Sanger sequencing confirmed product A to be reference transcript, and products D and E to contain the 89 bp aberrant exon as the intronic variant acted as an acceptor site. On translation, a stop codon is introduced after six amino acids into the aberrant exon. The product A present in patient fibroblasts reflects limited leakage of reference transcripts as a result of the two splice variants (c.119-2A>C and c.1100+1124G>A). Product B was determined to incorporate a novel aberrant 41 bp exon 581 bp downstream of the deep intronic variant (Figs. 1D, 1E), which is likely an alternate mis-spliced transcript. The ASO$_{NR2E3}$ transfected patient fibroblasts displayed an absence or decrease of two of the aberrantly exonized bands (loss of product E, decrease of product D) and a relative increase in reference band signal (product A) compared with the nontransfection condition (Fig. 1D). It is noted that ASO$_{NR2E3}$ transfected patient fibroblasts additionally displayed product C (268 bp), which was absent under nontransfection condition, and on Sanger sequencing confirmed an aberrant exonization.

Pedigree 2 (Complete Congenital Stationary Night Blindness)

Clinical Phenotype and Genetic Results. The proband is part of a sibship of five, born to consanguineous parents of Sudanese ancestry. The child had right exotropia since infancy, surgically corrected at 10 years of age. Night

blindness was first noted at 11 years of age, and his BCVA was 20/60 and 20/25 in the right and left eyes, respectively. He had high myopia and related fundus changes (Table 2; Figs. 5A, 5B). The SD-OCT was normal (Figs. 5C, 5D), ERG was consistent with selective ON-bipolar dysfunction (Fig. 5E; control traces are shown in Fig. 5F), and the clinical phenotype was consistent with the diagnosis of cCSNB. Both parents and all unaffected siblings had a normal eye exam including an ERG. Panel-based testing for CSNB (14 genes) in the proband did not identify any pathogenic variants.

GS Analysis of the six candidate genes known to cause cCSNB identified a homozygous intron 2 variant in *GPR179* (chr17:36494957:C>T; c.903+343G>A; NM_001004334.3; GRCh37/hg19), flagged by all *in silico* tools as a gain of function splice acceptor site 2 bp downstream (Table 1). SpliceAI annotation predicted an aberrant exon of 197 bp size with a start site at c.903+345 and a stop site at c.903+542 (Table 1; Figs. 2B, 2E). In gnomAD, this variant was recorded once in a heterozygous state (allele frequency of 3.187×10^{-5}) and never in a homozygous state. The variant segregated with the disease phenotype in the family (Fig. 2A). Supplementary Figure S2 lists two genes that carried homozygous coding variants that segregated with the disease but had no known human disease association and, hence, were not considered for further investigation.

Splicing Reporter Minigene RT-PCR and ASO Rescue. HEK293T cells were transfected with the following: GPR179:EMG:REF (reference sequence, c.903+343:G), GPR179:EMG:MT (variant sequence, c.903+343:A), and GPR179:EMG:MT + ASO$_{GPR179}$. RT-PCR of the reference clone (c.903+343:G) displayed two bands [products B (196 bp) and A (108 bp)] which upon Sanger sequencing confirmed to contain spliced exon 2, 3, and 4 or exon 2 and 4, respectively (Fig. 2C). The variant clone (c.903+343:A) displayed two distinct bands [product C (305 bp) and D (393 bp)]; Sanger sequencing confirmed both bands to incorporate the 197 bp aberrant exon as predicted by SpliceAI (Figs. 2C, 2E; Table 1). The variant clone cotransfected with ASO$_{GPR179}$ showed an abrogation in one of the two aberrant transcripts (abrogated product C but retained product D) and a gain in the reference transcript (product A; Fig. 2C). HEK293T cells with no transfection displayed no bands because *GPR179* expression levels are extremely low in nonneuronal tissue types.

Lymphoblast RT-PCR and ASO Rescue. In control lymphoblasts and ASO$_{GPR179}$ transfected control lymphoblasts, normal splicing of exon 2, 3, and 4 was confirmed on Sanger sequencing [Product B (196 bp); Fig. 2D]. In patient's lymphoblasts homozygous for c.903+343G>A, a different transcript (Product D [393 bp]; Fig. 2D) was identified; on Sanger sequencing this transcript was confirmed to have the 197 bp aberrant exon that introduced 44 amino acids and a premature stop. Hence, the deep intronic variant acted as an acceptor site for the existing exon 2 donor site. The reference transcript (product B) was not detected in the patient's lymphoblasts but did appear upon ASO$_{GPR179}$ transfection (Fig. 2D). A schematic for the observed transcripts is depicted in Figure 2E.

Pedigree 3 (Complete Achromatopsia)

Clinical Phenotype and Genetic Results. The proband, currently a 25-year-old male of Caucasian origin,
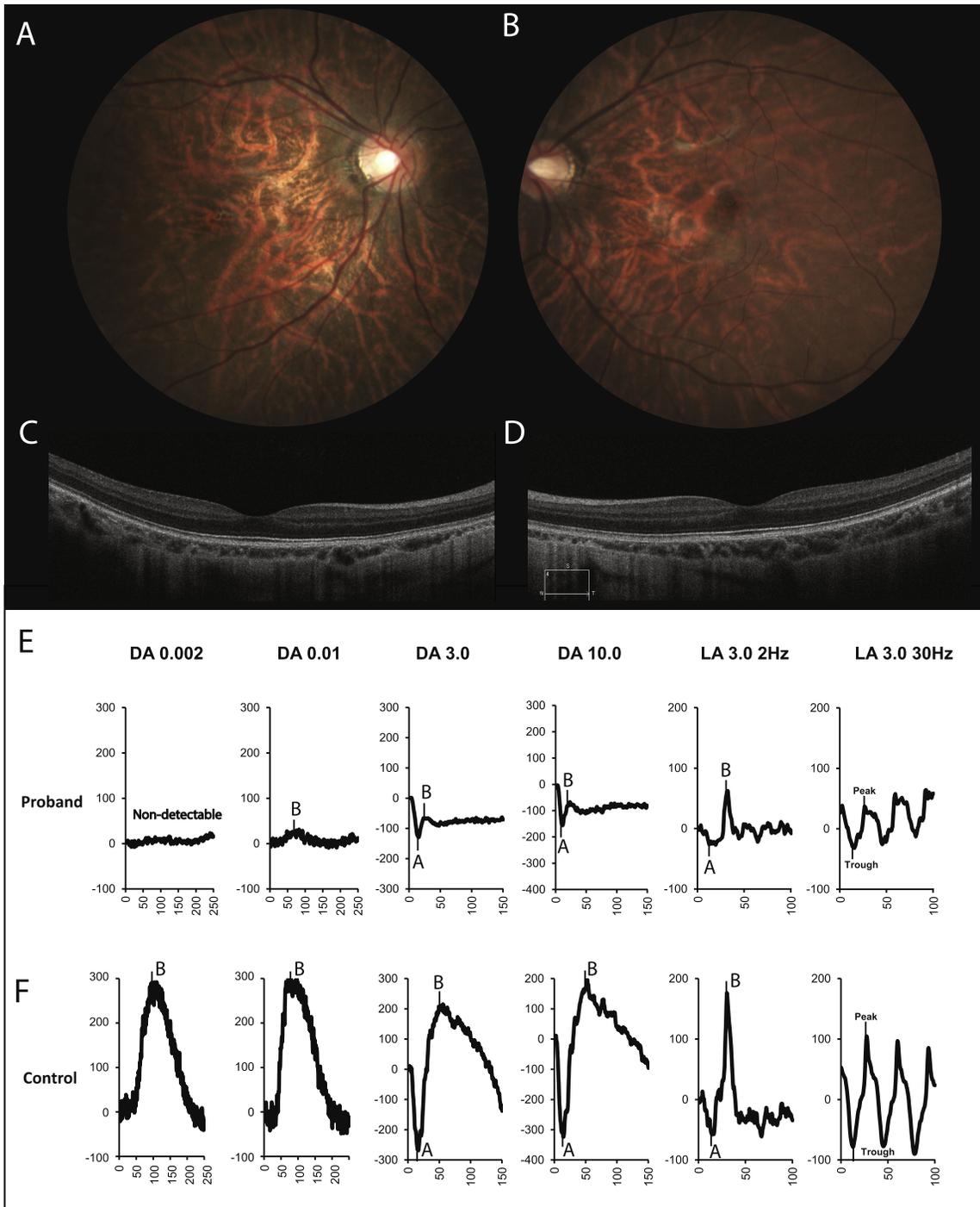
FIGURE 5. Clinical phenotype of Pedigree 2 proband. (**A, B**) Fundus images of the right and left eyes, respectively. Both eyes show tilted discs and temporal crescents, and the background retina is tessellated. (**C, D**) SD-OCT horizontal line scan across the center of the macula showed relatively preserved retinal thickness and layering. (**E**) ERG showed non-detectable response to dark adapted (DA) 0.002 cd.s.m^{-2} stimulus; DA 0.01 ERG showed markedly reduced b-wave amplitude. The DA 3.0 and DA 10.0 responses showed borderline a-wave amplitudes and electronegative configuration consistent with generalized rod ON-bipolar dysfunction. The light adapted (LA) 3.0 2Hz ERG showed broadened trough of the a-wave suggesting selective involvement of cone ON-bipolar system and the 30-Hz flicker responses showed low-normal amplitudes. (**F**) ERG responses from a control subject.

had nystagmus and photophobia since infancy. His BCVA has remained stable over time and was 20/200 in each eye at the most recent visit. He had high myopia and a strong color vision defect (Table 2). Fundus showed macular atrophy and AF showed foveal hyper auto-fluorescence (Table 2;

Figs. 6A, 6B). The SD-OCT showed bilateral grade 1 foveal hypoplasia and mild disruption of central macular photoreceptor outer segments (Table 2; Fig. 6C). The ERG results were consistent with complete ACHM (Fig. 6J); control traces are shown in Figure 6M.
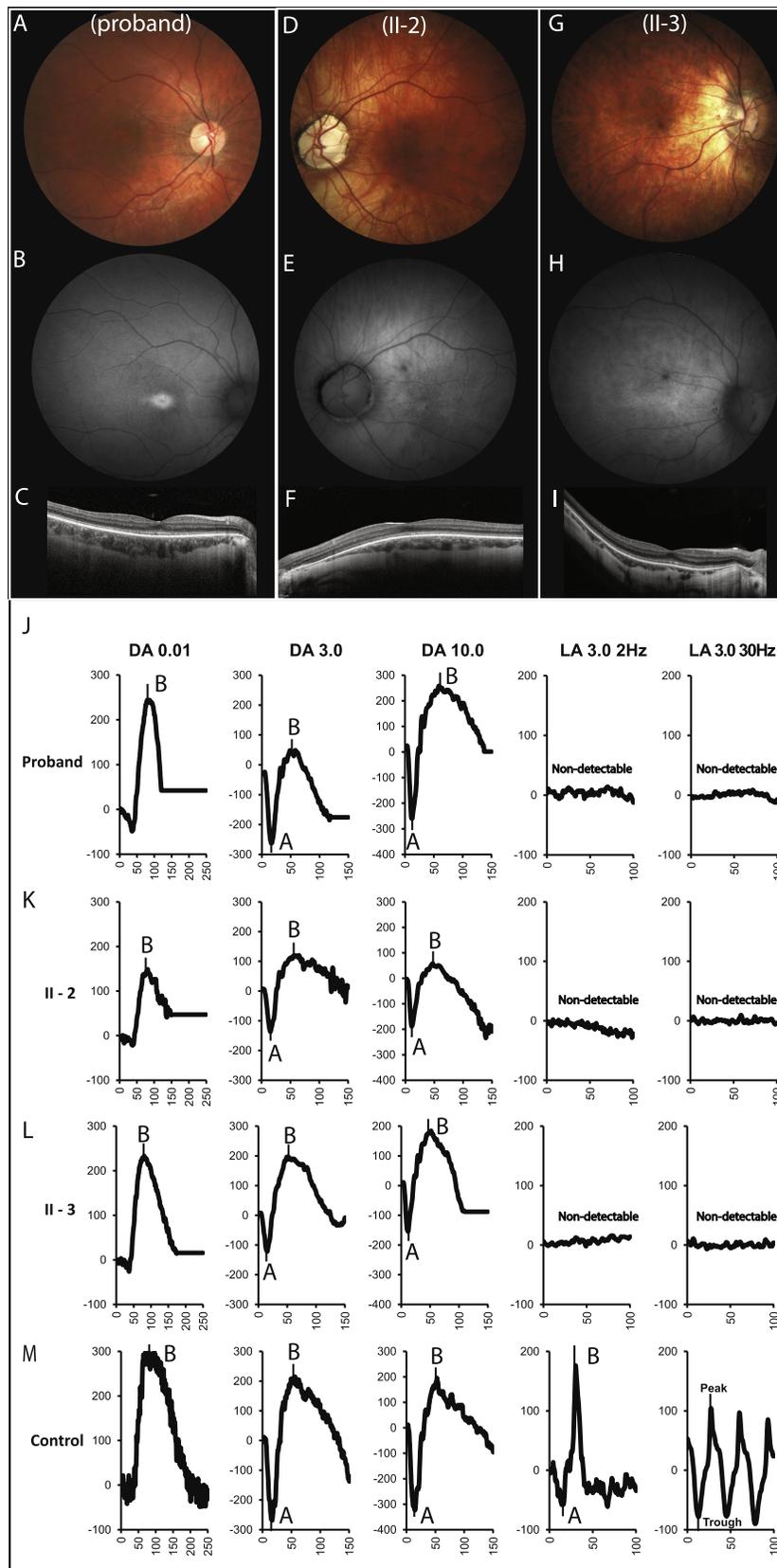
FIGURE 6. Detailed clinical phenotype in Pedigree 3. (**A, D, G**) The fundus image from one eye in each affected. The fundus in the proband (**A**) showed macular atrophy, whereas, both siblings showed tilted disc, peri-papillary atrophy and foveal hypoplasia (**D** and **G**). (**B, E, H**) Fundus autofluorescence (AF) images from the corresponding eye in each affected. The proband (**B**) showed marked foveal hyper-AF; II-2 showed subtle para-foveal hyper-AF; II-3 also showed subtle foveal hyper-AF (**H**). (**C, F, I**) are corresponding SD-OCT line scans from the central macula in the three cases. All SD-OCTs showed disruption of photoreceptor outer segments in the central macula; all cases

demonstrated Grade-1 foveal hypoplasia. (**J–L**) ERG traces from one eye of each affected individual showed dark adapted (DA) responses that were within normal limits and light adapted (LA) responses that were nondetectable above noise. The ERG findings were consistent with the clinical diagnosis of complete achromatopsia. (**M**) ERG responses from a control subject.

Two younger siblings (II-2 & II-3) also had symptoms of nystagmus and photophobia since infancy. At their most recent visit, the BCVA was 20/160 and 20/200 in the right and left eyes respectively, in II-2 (18 years), and 20/200 and 20/250 in the right and left eyes respectively, in II-3 (13 years). Both siblings also had high myopia and associated peripheral retinal changes (Table 2; Figs. 6D, 6G). The AF showed subtle increase in para-foveal (II-2) and foveal AF (II-3) (Table 2; Figs. 6E, 6H). Both siblings demonstrated bilateral grade 1 foveal hypoplasia, and mild central sub-foveal photoreceptor outer segment disruption on SD-OCT (Figs. 6F, 6I). The ERG was consistent with complete ACHM (Figs. 6K, 6L). Panel-based genetic testing identified a single heterozygous pathogenic variant in *CNGB3* in all three siblings (c.1148delC/p.Thr383Ilefs*13).[17]

GS analysis of candidate genes for ACHM revealed two variants in *CNGB3*; the previously identified exonic variant c.1148delC (p.Thr383Ilefs*13) and a deep intronic variant (intron 6; chr8:87674402:T>A; c.852+4751A>T; NM_019098.4; GRCh37/hg19), flagged by four of the five in silico splice algorithms to result in a gain of splice acceptor site at c.852+4756 and an aberrant 73 bp long exon (Table 1). If translated, a stop codon will be introduced after 2 amino acids into this aberrant exon. The intronic variant was not observed in gnomAD and the two *CNGB3* variants segregated with the disease phenotype in the pedigree (Fig. 3A). The c.1148delC is the most recurrent pathogenic variant reported in *CNGB3*.[8] A comprehensive analysis of GS did not reveal any other candidate gene with biallelic coding or canonical splice variants (Supplementary Fig. S3).

Splicing Reporter Minigene RT-PCR and ASO Rescue. HEK293T cells were transfected with the following: CNGB3:EMG:REF (reference sequence, c.852+4751:A), CNGB3:EMG:MT (variant sequence, c.852+4751:T), and CNGB3:EMG:MT + ASO$_{CNGB3}$. RT-PCR of the reference clone (c.852+4751:A) displayed a distinct band (product A [182 bp], Fig. 3C), which on Sanger sequencing contained the correctly spliced canonical exons 6 and 7. The variant clone (c.852+4751:T) displayed three distinct bands (products A, B, and C); on Sanger sequencing, product B (409 bp) incorporated an aberrant exon starting 5 bp downstream of the variant at the SpliceAI predicted acceptor site (Figs. 3C, 3D; Table 1). The aberrantly spliced exon did not pick up the SpliceAI predicted donor site. The product C (684 bp) was confirmed to be the unspliced minigene on Sanger sequencing (Figs. 3C, 3D). The variant clone co-transfected with ASO$_{CNGB3}$ showed an abrogation of product B (aberrant transcript) and presence of only product A (reference transcript; Fig. 3C).

Lymphoblast RT-PCR. Repeated attempts to amplify the cDNA from control and patient lymphoblast cell line were unsuccessful due to the poor expression of *CNGB3* outside the retina, and this challenge has been reported previously.[8]

DISCUSSION

This study reports the solving of three distinct IRDs by following a similar principle of integrating knowledge from deep phenotyping and its application to GS analysis. Three novel deep intronic splice mutations leading to inclusion of an aberrant exon by way of a gain-of-function splice acceptor site were identified in three different cases of IRDs; ESCS, cCSNB, and complete ACHM. These are the first documented pathogenic deep intronic mutational events in *NR2E3* and *GPR179*, genes that are always associated with specific phenotypes ESCS and cCSNB, respectively.[15,16,42] Precise phenotyping guided the targeted assessment of GS, that led to mutational discovery in each instance. Functional assay using splice reporter minigene constructs and/or patient-derived cell lines confirmed mutation pathogenicity as predicted by in silico tools.

Enhanced S-cone syndrome (ESCS) is a condition where the electrophysiological phenotype is pathognomonic of mutations in *NR2E3* or *NRL*.[42–45] The proband's ERG (Pedigree 1) demonstrated these characteristic features that reflected the underlying anatomical defect of a rod-devoid retina with all detectable ERG responses being dominated by an excess of S-cones that cannot respond well to a fast flicker stimulus; the specific molecular mechanisms are poorly understood.[46,47] It is noted that although the proband displayed night blindness, retinal findings were subtle and did not include the foveal schisis or nummular pigmentation often associated with ESCS.[44,48] Furthermore, the proband's SD-OCT demonstrated characteristic retinal rosettes previously described in the rd7 mouse model mutant for *Nr2e3*[49] and human patients with *NR2E3*-related ESCS (Vincent, A, IOVS, 2013, 54, 15, ARVO E-Abstract). The identification of a known pathogenic variant in *NR2E3* (c.119-2A>C)[14] on panel-based sequencing and the precise phenotypic information guided the identification of the deep intronic variant (c.1100+1124G>A) by GS which was further validated by segregation and functional assays. The presence of some amount of reference NR2E3 transcript in the patient cDNA experiments due to leaky splicing of the two splice variants may account for the milder fundus findings in the proband; the c.119-2A>C variant assays (minigene) has been earlier reported to cause incomplete skipping of exon 2 of *NR2E3* leading to some retention of the reference transcript.[43]

Complete CSNB (cCSNB), a usually non-progressive disorder, is genetically heterogeneous but is defined by characteristic features that include night blindness, high refractive error, largely normal retinal appearance, and selective retinal ON-bipolar cell dysfunction (rods and cones) on ERG. The proband in Pedigree-2 displayed these characteristic features.[50] Panel-based gene analysis failed to identify any exonic variants in the known CSNB genes.[50,51] The GS analysis prioritizing cCSNB genes identified a homozygous *GPR179* variant (c.903+343G>A) that was validated using segregation analysis, splicing reporter minigene assay, and patient-derived lymphoblasts.

Complete ACHM is a severe form of largely nonprogressive cone dysfunction syndrome that encompasses clinical features of infantile onset nystagmus and photophobia, reduced vision, severe color vision deficiency, normal retinal appearance, and non-detectable photopic ERGs; the proband and affected siblings in Pedigree-3 demonstrated these phenotypic features.[52] Panel-based clinical testing

revealed the previously reported most common pathogenic variant (c.1148delC) in *CNGB3*; this variant results in the introduction of a premature stop codon.[8,17,53] Targeted GS analysis in candidate genes identified a deep intronic second variant in *CNGB3* (c.852+4751A>T) that strongly predicted to cause aberrant exonization, and the variants segregated with the disease phenotype. A splicing reporter minigene assay confirmed the occurrence of aberrant exonization consequent to the deep intronic mutation. A recent publication identified three additional deep intronic splice variants in *CNGB3* in a large cohort of achromatopsia.[8]

In recent years, deep intronic variants have increasingly accounted for missing heritability in several IRDs.[3–9] In *ABCA4*-retinopathy, amongst cases with one known pathogenic allele, deep intronic variants accounted as the second allele for between 10% to 50% of cases; a recent study reported deep intronic pathogenic variants in 20% of their cohort with one recurrent mutation occurring in 2.6% of their entire *ABCA4*-cohort.[54–59] A deep intronic variant in *CNGB3* (c.1663-1205G>A) was reported to be the eighth most recurring pathogenic allele in the gene in a large cohort.[8] Although the current study prioritized a targeted gene panel approach, we also explored the GS in detail and excluded any probable novel gene associations in all cases. Hence, targeted analysis for identifying deep intronic variants in known genes with a well-established phenotype should be considered before exploring novel gene associations in unsolved cases of IRDs; this may be even more relevant in AR IRD cases with a known heterozygous pathogenic allele.

In this study, the pathogenicity of deep intronic variants was predicted through Alamut's Visual software (four in silico splice tools) and Illumina SpliceAI. Based on a deep neural network, SpliceAI aims to predict splice junctions from arbitrary pre-mRNA transcript sequences and generates anticipated start and end positions of aberrant exons with the greatest accuracy.[33,60] All deep intronic variants had significant splicing scores in at least four of the five *in silico* tools and predicted a novel 3′ acceptor site in a region where an existing branch point sequence, polypyrimidine tract sequence, and 5′ donor site was favorable for the spliceosome to generate an aberrant exon with a premature stop.[10,11] In all cases, the start of the aberrant exon began after the dinucleotide "AG" and a premature stop codon were noted after six (*NR2E3*), forty-four (*GPR179*) and two amino acids (*CNGB3*), respectively. In fact, in two instances (*NR2E3* and *GPR179*), the predicted length of the aberrant exon by SpliceAI matched the observed length of the aberrant exon in the minigene system and/or cell line experiments. In the *CNGB3* minigene assay, aberrant exonization occurred at the predicted acceptor site (SpliceAI, 5 bp downstream of variant), but the system did not use the predicted donor site within the minigene intron, and therefore the resultant product was longer than predicted.

Although patient-derived cDNA or minigene experiments validated the aberrant splicing effect of all three deep intronic variants identified, there was a discrepancy in the splice product size observed between patient cDNA analyses and minigene assays for two variants (*NR2E3* and *GPR179*). This discrepancy has been previously observed in the literature (including in *CDH23*)[61–63] and is believed to be due to differences in expression of splice factors and splice regulatory factors in different cell types or to the methodologic constraints that limit the minigene construct length to a few exons (1 or 2).[64–66] The shorter size of the minigene intron

unit within the *CNGB3* construct (644 bp) compared with intron 6 of the genomic DNA (12,869 bp) likely prevented the inclusion of the aberrant exon that occurs in vivo. Splicing machinery is influenced by the genomic context where higher fidelity splicing outcomes are more likely with larger genomic DNA.[61,65] Hence, using patient-derived cell lines is advantageous in that this system likely better recapitulates the in vivo context but might not be available or suitable in all instances.[8,10,63] Furthermore, for genes such as *NR2E3*, *GPR179*, and *CNGB3* that are expressed almost exclusively in the retina, it can be challenging to detect transcript levels in nonnative tissue types like fibroblasts or lymphoblasts cell lines.[67,68] In these instances, splice reporting minigene or modified minigene constructs are a more feasible approach to validate aberrant splicing.[10,63]

ASOs are synthetic analogues of single stranded RNA or DNA with unique chemical structure. These molecules are typically 15 to 30 bp in length and can be designed to bind to a site of interest with high specificity to modulate splicing of pre-mRNA transcripts.[69] Deep intronic variants act through the gain of an aberrant exon that shifts the frame of the transcript out of frame and/or adds premature stop codons that trigger nonsense mediated decay.[10,12] A stable ASO specific for the essential splicing motif in the deep intron can cause this aberrant exon to be skipped thus restoring the normal splicing reaction and recovering normal product.[70] The RNA-based ASOs used in this study caused moderate restoration of the reference transcript while partially or completely abrogating the aberrantly exonized transcripts in all three cases. ASOs are increasingly playing a role in emerging novel precision clinical treatments. Several clinical trials are underway for testing the efficacy of ASOs in neurologic diseases such as Duchenne muscular dystrophy and spinal muscular atrophy, and for a specific *CEP290*-related IRD (NCT03140969).[69] Moreover, the splicing abnormalities caused by the deep intronic variants in *ABCA4* and *USH2A* have all been shown to be rescued by ASO treatment ex vivo.[3,4,71] With evolving discoveries of deep intronic variants explaining the genotype in multiple IRDs, ASO-mediated therapies for IRDs will increase.

In summary, the analytical and bioinformatics tools currently available for GS allow for improved analysis of noncoding regions of the genome and enhance our capability to detect deep intronic mutational events. Combining deep phenotyping with targeted GS analysis can accelerate detection of these deep intronic variants that account in part for missing heritability in IRDs.

Acknowledgments

References

1. Weisschuh N, Mayer AK, Strom TM, et al. Mutation detection in patients with retinal dystrophies using targeted next generation sequencing. *PLoS One*. 2016;11:e0145951.

2. Weisschuh N, Obermaier CD, Battke F, et al. Genetic architecture of inherited retinal degeneration in Germany: a large cohort study from a single diagnostic center over a 9-year period [published online ahead of print]. *Hum Mutat*, https://doi.org/10.1002/humu.24064.

3. Bauwens M, Garanto A, Sangermano R, et al. ABCA4-associated disease as a model for missing heritability in autosomal recessive disorders: novel noncoding splice, cis-regulatory, structural, and recurrent hypomorphic variants. *Genet Med*. 2019;21:1761–1771.

4. Sangermano R, Garanto A, Khan M, et al. Deep-intronic ABCA4 variants explain missing heritability in Stargardt disease and allow correction of splice defects by antisense oligonucleotides. *Genet Med*. 2019;21:1751–1760.

5. den Hollander AI, Koenekoop RK, Yzer S, et al. Mutations in the CEP290 (NPHP6) gene are a frequent cause of Leber congenital amaurosis. *Am J Hum Genet*. 2006;79:556–561.

6. Liquori A, Vache C, Baux D, et al. Whole USH2A gene sequencing identifies several new deep intronic mutations. *Hum Mutat*. 2016;37:184–193.

7. Khan AO, Becirovic E, Betz C, et al. A deep intronic CLRN1 (USH3A) founder mutation generates an aberrant exon and underlies severe Usher syndrome on the Arabian Peninsula. *Sci Rep*. 2017;7:1411.

8. Weisschuh N, Sturm M, Baumann B, et al. Deep-intronic variants in CNGB3 cause achromatopsia by pseudoexon activation. *Hum Mutat*. 2020;41:255–264.

9. Zeitz C, Michiels C, Neuille M, et al. Where are the missing gene defects in inherited retinal disorders? Intronic and synonymous variants contribute at least to 4% of CACNA1F-mediated inherited retinal disorders. *Hum Mutat*. 2019;40:765–787.

10. Anna A, Monika G. Splicing mutations in human genetic disorders: examples, detection, and confirmation. *J Appl Genet*. 2018;59:253–268.

11. Scotti MM, Swanson MS. RNA mis-splicing in disease. *Nat Rev Genet*. 2016;17:19–32.

12. Vaz-Drago R, Custodio N, Carmo-Fonseca M. Deep intronic mutations and human disease. *Hum Genet*. 2017;136:1093–1111.

13. Hsu MK, Lin HY, Chen FC. NMD Classifier: a reliable and systematic classification tool for nonsense-mediated decay events. *PLoS One*. 2017;12:e0174798.

14. Haider NB, Jacobson SG, Cideciyan AV, et al. Mutation of a nuclear receptor gene, NR2E3, causes enhanced S cone syndrome, a disorder of retinal cell fate. *Nat Genet*. 2000;24:127–131.

15. Audo I, Bujakowska K, Orhan E, et al. Whole-exome sequencing identifies mutations in GPR179 leading to autosomal-recessive complete congenital stationary night blindness. *Am J Hum Genet*. 2012;90:321–330.

16. Peachey NS, Ray TA, Florijn R, et al. GPR179 is required for depolarizing bipolar cell function and is mutated in autosomal-recessive complete congenital stationary night blindness. *Am J Hum Genet*. 2012;90:331–339.

17. Kohl S, Baumann B, Broghammer M, et al. Mutations in the CNGB3 gene encoding the beta-subunit of the cone photoreceptor cGMP-gated channel are responsible for achromatopsia (ACHM3) linked to chromosome 8q21. *Hum Mol Genet*. 2000;9:2107–2116.

18. McCulloch DL, Marmor MF, Brigell MG, et al. ISCEV Standard for full-field clinical electroretinography (2015 update). *Doc Ophthalmol*. 2015;130:1–12.

19. Tavares E, Tang CY, Vig A, et al. Retrotransposon insertion as a novel mutational event in Bardet-Biedl syndrome. *Mol Genet Genomic Med* 2019;7:e00521.

20. Lionel AC, Costain G, Monfared N, et al. Improved diagnostic yield compared with targeted gene sequencing panels suggests a role for whole-genome sequencing as a first-tier genetic test. *Genet Med*. 2018;20:435–443.

21. Li H, Durbin R. Fast and accurate long-read alignment with Burrows-Wheeler transform. *Bioinformatics*. 2010;26:589–595.

22. McKenna A, Hanna M, Banks E, et al. The Genome Analysis Toolkit: a MapReduce framework for analyzing next-generation DNA sequencing data. *Genome Res*. 2010;20:1297–1303.

23. Wang K, Li M, Hakonarson H. ANNOVAR: functional annotation of genetic variants from high-throughput sequencing data. *Nucleic Acids Res*. 2010;38:e164.

24. Thung DT, de Ligt J, Vissers LE, et al. Mobster: accurate detection of mobile element insertions in next generation sequencing data. *Genome Biol*. 2014;15:488.

25. Zhang ZD, Du J, Lam H, et al. Identification of genomic indels and structural variations using split reads. *BMC Genomics*. 2011;12:375.

26. Zhu M, Need AC, Han Y, et al. Using ERDS to infer copy-number variants in high-coverage genomes. *Am J Hum Genet*. 2012;91:408–421.

27. Moran J, K GS, Maynes J, et al. IFT80 mutations cause a novel complex ciliopathy phenotype with retinal degeneration. *Clin Genet*. 2018;94:368–372.

28. Vincent A, Ng J, Gerth-Kahlert C, et al. Biallelic mutations in CRB1 underlie autosomal recessive familial foveal retinoschisis. *Invest Ophthalmol Vis Sci*. 2016;57:2637–2646.

29. Desmet FO, Hamroun D, Lalande M, Collod-Beroud G, Claustres M, Beroud C. Human Splicing Finder: an online bioinformatics tool to predict splicing signals. *Nucleic Acids Res*. 2009;37:e67.

30. Eng L, Coutinho G, Nahas S, et al. Nonclassical splicing mutations in the coding and noncoding regions of the ATM Gene: maximum entropy estimates of splice junction strengths. *Hum Mutat*. 2004;23:67–76.

31. Reese MG, Eeckman FH, Kulp D, Haussler D. Improved splice site detection in Genie. *J Comput Biol*. 1997;4:311–323.

32. Pertea M, Lin X, Salzberg SL. GeneSplicer: a new computational method for splice site prediction. *Nucleic Acids Res* 2001;29:1185–1190.

33. Jaganathan K, Kyriazopoulou Panagiotopoulou S, McRae JF, et al. Predicting splicing from primary sequence with deep learning. *Cell*. 2019;176:535–548 e524.

34. Bergsma AJ, In 't Groen SL, Verheijen FW, van der Ploeg AT, Pijnappel W. From cryptic toward canonical pre-mRNA splicing in Pompe disease: a pipeline for the development of antisense oligonucleotides. *Mol Ther Nucleic Acids*. 2016;5:e361.

35. Gaildrat P, Killian A, Martins A, Tournier I, Frebourg T, Tosi M. Use of splicing reporter minigene assay to evaluate the

effect on splicing of unclassified genetic variants. *Methods Mol Biol*. 2010;653:249–257.

36. Wilson AM, Schlade-Bartusiak K, Tison JL, Macintyre G, Cox DW. A minigene approach for analysis of ATP7B splice variants in patients with Wilson disease. *Biochimie*. 2009;91:1342–1345.

37. Fraile-Bethencourt E, Valenzuela-Palomo A, Diez-Gomez B, Caloca MJ, Gomez-Barrero S, Velasco EA. Minigene splicing assays identify 12 spliceogenic variants of BRCA2 exons 14 and 15. *Front Genet*. 2019;10:503.

38. Zhao J, Sun Y, Huang Y, et al. Functional analysis reveals that RBM10 mutations contribute to lung adenocarcinoma pathogenesis by deregulating splicing. *Sci Rep*. 2017;7:40488.

39. Costantino L, Rusconi D, Solda G, et al. Fine characterization of the recurrent c.1584+18672A>G deep-intronic mutation in the cystic fibrosis transmembrane conductance regulator gene. *Am J Respir Cell Mol Biol*. 2013;48:619–625.

40. Kole R, Krainer AR, Altman S. RNA therapeutics: beyond RNA interference and antisense oligonucleotides. *Nat Rev Drug Discov*. 2012;11:125–140.

41. Scoles DR, Minikel EV, Pulst SM. Antisense oligonucleotides: A primer. *Neurol Genet*. 2019;5:e323.

42. Vincent A, Robson AG, Holder GE. Pathognomonic (diagnostic) ERGs. A review and update. *Retina*. 2013;33:5–12.

43. Bernal S, Solans T, Gamundi MJ, et al. Analysis of the involvement of the NR2E3 gene in autosomal recessive retinal dystrophies. *Clin Genet*. 2008;73:360–366.

44. Audo I, Michaelides M, Robson AG, et al. Phenotypic variation in enhanced S-cone syndrome. *Invest Ophthalmol Vis Sci*. 2008;49:2082–2093.

45. Littink KW, Stappers PTY, Riemslag FCC, et al. Autosomal recessive NRL mutations in patients with enhanced S-cone syndrome. *Genes (Basel)*. 2018;9:68.

46. Milam AH, Rose L, Cideciyan AV, et al. The nuclear receptor NR2E3 plays a role in human retinal photoreceptor differentiation and degeneration. *Proc Natl Acad Sci USA*. 2002;99:473–478.

47. Mollema N, Haider NB. Focus on molecules: nuclear hormone receptor Nr2e3: impact on retinal development and disease. *Exp Eye Res*. 2010;91:116–117.

48. Marmor MF, Jacobson SG, Foerster MH, Kellner U, Weleber RG. Diagnostic clinical findings of a new syndrome with night blindness, maculopathy, and enhanced S cone sensitivity. *Am J Ophthalmol* 1990;110:124–134.

49. Haider NB, Naggert JK, Nishina PM. Excess cone cell proliferation due to lack of a functional NR2E3 causes retinal dysplasia and degeneration in rd7/rd7 mice. *Hum Mol Genet*. 2001;10:1619–1626.

50. Zeitz C, Robson AG, Audo I. Congenital stationary night blindness: an analysis and update of genotype-phenotype correlations and pathogenic mechanisms. *Prog Retin Eye Res*. 2015;45:58–110.

51. Vincent A, Audo I, Tavares E, et al. Biallelic mutations in GNB3 cause a unique form of autosomal-recessive congenital stationary night blindness. *Am J Hum Genet*. 2016;98:1011–1019.

52. Michaelides M, Hunt DM, Moore AT. The cone dysfunction syndromes. *Br J Ophthalmol*. 2004;88:291–297.

53. Kohl S, Jagle H, Wissinger B, Zobor D. Achromatopsia. In: Ardinger HH, Pagon RA , et al., eds. GeneReviews. Seattle (WA)1993.

54. Zernant J, Xie YA, Ayuso C, et al. Analysis of the ABCA4 genomic locus in Stargardt disease. *Hum Mol Genet* 2014;23:6797–6806.

55. Bauwens M, De Zaeytijd J, Weisschuh N, et al. An augmented ABCA4 screen targeting noncoding regions reveals a deep intronic founder variant in Belgian Stargardt patients. *Hum Mutat* 2015;36:39–42.

56. Bax NM, Sangermano R, Roosing S, et al. Heterozygous deep-intronic variants and deletions in ABCA4 in persons with retinal dystrophies and one exonic ABCA4 variant. *Hum Mutat* 2015;36:43–47.

57. Braun TA, Mullins RF, Wagner AH, et al. Non-exomic and synonymous variants in ABCA4 are an important cause of Stargardt disease. *Hum Mol Genet* 2013;22:5136–5145.

58. Schulz HL, Grassmann F, Kellner U, et al. Mutation spectrum of the ABCA4 gene in 335 Stargardt disease patients from a multicenter German cohort-impact of selected deep intronic variants and common SNPs. *Invest Ophthalmol Vis Sci* 2017;58:394–403.

59. Nassisi M, Mohand-Said S, Andrieu C, et al. Prevalence of ABCA4 deep-intronic variants and related phenotype in an unsolved "one-hit" cohort with Stargardt disease. *Int J Mol Sci* 2019;20:5053

60. Wai HA, Lord J, Lyon M, et al. Blood RNA analysis can increase clinical diagnostic rate and resolve variants of uncertain significance. *Genet Med*. 2020;22:1005–1014.

61. Aparisi MJ, Garcia-Garcia G, Aller E, et al. Study of USH1 splicing variants through minigenes and transcript analysis from nasal epithelial cells. *PLoS One*. 2013;8:e57506.

62. Acedo A, Sanz DJ, Duran M, et al. Comprehensive splicing functional analysis of DNA variants of the BRCA2 gene by hybrid minigenes. *Breast Cancer Res*. 2012;14:R87.

63. van der Klift HM, Jansen AM, van der Steenstraten N, et al. Splicing analysis for exonic and intronic mismatch repair gene variants associated with Lynch syndrome confirms high concordance between minigene assays and patient RNA analyses. *Mol Genet Genomic Med*. 2015;3:327–345.

64. Baralle M, Skoko N, Knezevich A, et al. NF1 mRNA biogenesis: effect of the genomic milieu in splicing regulation of the NF1 exon 37 region. *FEBS Lett*. 2006;580:4449–4456.

65. Buratti E, Baralle M, Baralle FE. Defective splicing, disease and therapy: searching for master checkpoints in exon definition. *Nucleic Acids Res*. 2006;34:3494–3510.

66. Weisschuh N, Buena-Atienza E, Wissinger B. Splicing mutations in inherited retinal diseases. *Prog Retin Eye Res*. 2020:100874.

67. Pinelli M, Carissimo A, Cutillo L, et al. An atlas of gene expression and gene co-regulation in the human retina. *Nucleic Acids Res*. 2016;44:5773–5784.

68. Mele M, Ferreira PG, Reverter F, et al. Human genomics. The human transcriptome across tissues and individuals. *Science*. 2015;348:660–665.

69. Rinaldi C, Wood MJA. Antisense oligonucleotides: the next frontier for treatment of neurological disorders. *Nat Rev Neurol* 2018;14:9–21.

70. Havens MA, Hastings ML. Splice-switching antisense oligonucleotides as therapeutic drugs. *Nucleic Acids Res* 2016;44:6549–6563.

71. Slijkerman RW, Vache C, Dona M, et al. Antisense oligonucleotide-based splice correction for USH2A-associated retinal degeneration caused by a frequent deep-intronic mutation. *Mol Ther Nucleic Acids* 2016;5:e381.